Strong environmental coupling in a Josephson parametric amplifier

J. Y. Mutus,[1,a)] T. C. White,[1,a)] R. Barends,[1] Yu Chen,[1] Z. Chen,[1] B. Chiaro,[1] A. Dunsworth,[1] E. Jeffrey,[1] J. Kelly,[1] A. Megrant,[1,2] C. Neill,[1] P. J. J. O'Malley,[1] P. Roushan,[1] D. Sank,[1] A. Vainsencher,[1] J. Wenner,[1] K. M. Sundqvist,[3] A. N. Cleland,[1] and John M. Martinis[1,b)]
[1]*Department of Physics, University of California, Santa Barbara, California 93106-9530, USA*
[2]*Department of Materials, University of California, Santa Barbara, California 93106, USA*
[3]*Department of Electrical and Computer Engineering, Texas A&M University, College Station, Texas 77843, USA*

(Received 22 May 2014; accepted 19 June 2014; published online 2 July 2014)

We present a lumped-element Josephson parametric amplifier designed to operate with strong coupling to the environment. In this regime, we observe broadband frequency dependent amplification with multi-peaked gain profiles. We account for this behavior using the "pumpistor" model which allows for frequency dependent variation of the external impedance. Using this understanding, we demonstrate control over the complexity of gain profiles through added variation in the environment impedance at a given frequency. With strong coupling to a suitable external impedance, we observe a significant increase in dynamic range, and large amplification bandwidth up to 700 MHz giving near quantum-limited performance. © *2014 AIP Publishing LLC*.
[http://dx.doi.org/10.1063/1.4886408]

Parametric amplification is a result of frequency mixing via a nonlinear element coupled to an external environment. Amplifiers based on this principle have achieved near quantum limited performance,[1] essential for high fidelity measurement of both optical[2] and microwave[3,4] signals. In the microwave domain, the Josephson parametric amplifier[5–10] (JPA) has enabled new studies of quantum jumps[11] and measurement of quantum trajectories.[12] While well suited to single qubit dynamics, progress in scaling to larger quantum algorithms and fault-tolerant quantum computing[13–15] is limited by JPA bandwidth and dynamic range. JPA performance is constrained by weak coupling between the nonlinear resonator and the environment, chosen to simplify amplifier dynamics.

In this Letter, we experimentally demonstrate a JPA operated in a previously unreported regime of strong coupling to the environment. Physical insight into this coupling interaction follows naturally from the "pumpistor" model of a flux driven superconducting quantum interference device (SQUID), previously used to describe only degenerate (phase-sensitive) amplification.[16] By adapting the non-degenerate (phase-preserving) "pumpistor" theory,[17] we create a model which accounts for dramatic improvements in both quantum limited bandwidth and dynamic range observed in this device. Additionally, by varying the environment we demonstrate significant control over amplifier dynamics and provide a further verification of the full "pumpistor" theory.

The JPA relies on the Josephson inductance to create a nonlinear resonator which is typically weakly coupled to a 50 Ω embedding environment. When driven by a pump tone of sufficient power, energy is coupled from the pump (ω_p) into other signals within the resonator bandwidth. A signal applied near the resonant frequency (ω_o) results in an amplified signal (ω_s) and idler (ω_i) tone. In this work, the amplifier is operated as a non-degenerate (phase-preserving) three-wave mixing amplifier, where $\omega_p = \omega_s + \omega_i$ and $\omega_p \approx 2\omega_o$. The amplifier operates in a reflection mode where a microwave circulator separates the incoming signal from the outgoing amplified signal and idler tones, which are further amplified by a cryogenic following amplifier, typically a high-electron mobility transistor (HEMT) amplifier.[18]

The impedance-transformed parametric amplifier (IMPA) shown in Fig. 1 builds on a typical lumped-element style JPA consisting of a SQUID loop with 100 pH of combined geometric and non-linear (Josephson) inductance L_j shunted by a 4 pF parallel plate capacitor C, for a characteristic impedance of $1/\omega_o C \approx 5\,\Omega$. Typically, this resonator is coupled to a 50 Ω transmission line, either directly or with a coupling capacitor. Practical measurements with the JPA are limited by narrow bandwidth (10–20 MHz typ.) and the low signal power (−120 dBm typ.) at which the amplifier saturates. These figures of merit are many orders of magnitude lower than the HEMT following amplifier. Bandwidth in the JPA scales as $1/Q$ and saturation power scales as I_c^2/Q,[19] where I_c is the critical current of the SQUID and $Q = Z_o\omega_o C = Z_o/\omega_o L$ is the low power coupled Q of the JPA. For a fixed environment impedance Z_o and frequency ω_o, the coupled Q and critical current cannot be varied independently because $L_j \propto 1/I_c$, introducing trade-offs between saturation power and bandwidth. This trade off can be circumvented using multiple SQUIDS in series,[20] but this makes fabrication less reliable and complicates device operation.

In the IMPA, we instead transform the environmental impedance Z_o, increasing coupling, lowering Q and thus simultaneously increasing the bandwidth and saturation power. We use a tapered impedance transformer (Fig. 1) to lower the effective external impedance seen by the JPA from 50 Ω to about 15 Ω. In this way, we can directly probe the effects of lowering the coupled Q while at the same time increasing both saturation power and available bandwidth.

[a)]J. Y. Mutus and T. C. White contributed equally to this work.
[b)]martinis@physics.ucsb.edu

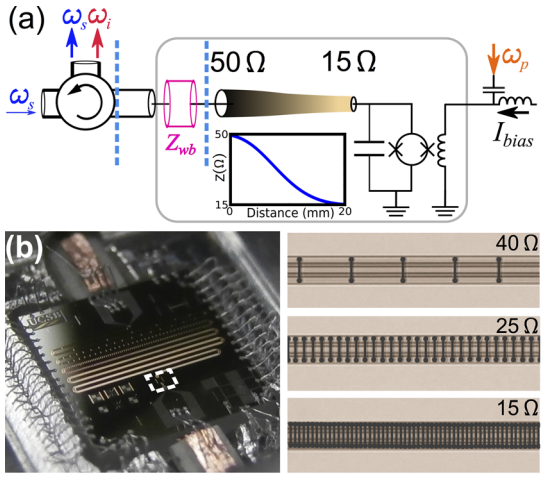

FIG. 1. Schematic and photograph of the IMPA. (a) Circuit diagram of the IMPA (gray, light box) and accessory microwave hardware. The device consists of a nonlinear LC resonant circuit coupled to the 50 Ω environment by a tapered transmission line, smoothly varying from 50 Ω to 15 Ω, with profile shown in the inset. The bias port (right) injects current I_{bias} to change the resonant frequency ω_o of the circuit by varying the inductance of the SQUID loop. Dominant sources of reflections (dashed blue lines) in the chain are the circulator, used to separate incoming and amplified outgoing signals, and the wire-bond (pink, light) shown as Z_{wb}. (b) Photograph of device. The chip is a 3 mm × 3 mm square. The gradient of the crossover density is visible as the 20 mm long CPW becomes increasingly bronze (light) in color. The LC resonant circuit is contained within the dashed box. On the right are photo-micrographs of different regions of the hybrid CPW/microstrip transmission line. As the density of 2 μm wide crossovers (false color in black) increases, the impedance of the transmission line drops.

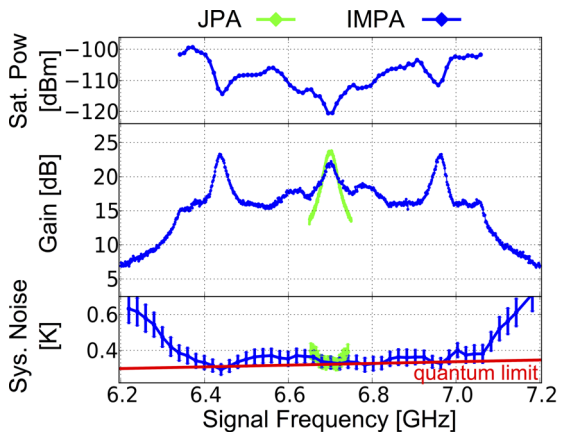

FIG. 2. Input saturation power, gain, and noise performance of the IMPA. Here, we show amplifier performance centered at 6.7 GHz for a single pump tone at 13.4 GHz. The IMPA (blue, dark) provides an average input saturation power (defined as 1 dB compression point) of −108 dBm with regions as high as −103 dBm. The device gives greater than 15 dB of gain and near quantum-limited performance over a bandwidth of nearly 700 MHz. This is compared to a typical JPA with a $Q = 10$ (green, light) for a similar gain, which only provides quantum-limited performance over a 60 MHz band. We define the quantum limit as one photon $\hbar\omega$ of total system noise at the input of the amplifier. Here, deviations from the quantum noise limit correspond to gains that are unable to completely overwhelm the noise added by the HEMT following amplifier. Error bars on the noise correspond to potential systemic calibration errors on HEMT system noise.

A hybrid geometry was adopted for the taper, since the 15 Ω to 50 Ω impedance range is not intrinsically suited to either a purely co-planar waveguide (CPW) or microstrip transmission line. The tapered line consists of a fixed geometry CPW shunted with parallel plate capacitor cross-overs. The sections with a cross-over approximate a microstrip transmission line, with much lower local characteristic impedance. The small size of the crossovers (2 μm) relative to the wavelength of a 6 GHz photon, allows us to vary the impedance smoothly with the density of crossovers, following a 20 mm long Klopfenstein taper,[21,22] a profile chosen to minimize the pass-band ripple of the network; see Fig. 1.[23]

Using this new device we measure a significant increase in average saturation power, the power at which the gain compresses by 1 dB, with values as high as −103 dBm at 15 dB gain, as shown in Fig. 2. Decreasing the coupled Q has the added benefit of increasing bandwidth. We have measured amplification bandwidths of nearly 700 MHz, shown in Fig. 2 for data centered about 6.7 GHz. Due to the multi-peaked gain features visible in the figure, we define the amplification bandwidth as the frequency range over which the device approaches the quantum noise limit. We calculate system noise using the method of signal to noise ratio improvement[8,10] over the calibrated noise of the HEMT following amplifier. Further information on the HEMT noise measurement can be found in the supplement.[23]

The increase in average saturation power up to −108 dBm is consistent with theoretical expectations coming from both lower coupled Q (about 5 dB increase) and lower average gain (about 2–3 dB increase). This increase in input saturation power allows the amplifier to amplify both a higher power signal as well as quantum fluctuations from a larger bandwidth.[23] The factor of 10 improvement in the bandwidth, however, cannot be explained by the reduced coupled Q. Moreover, the shape of the gain profile differs significantly from the typical Lorentzian described by most resonant JPA models[19,20,24] and thus requires a detailed understanding of how the JPA interacts with variations in the microwave environment.

For a JPA coupled to a perfect 50 Ω environment, the incident signal tone at ω_s reflects off the LC resonator, where pump photons are converted to amplified signal ω_s and idler ω_i tones. In the case of an imperfect match to the environment, the outgoing amplified signal and idler tones are back-reflected towards the JPA, creating standing waves and affecting device gain through constructive or destructive interference. These standing waves are properly thought of as variations in the frequency dependent admittance $Y_{\text{ext}}(\omega_s)$ (inverse impedance) of the environment seen by the JPA. The predominant sources of reflections in the microwave chain are due to the wire-bond and microwave circulator interfaces, shown as dashed lines in Fig. 1(a). Typically, experiments are designed to minimize the distance between the JPA and these reflection planes, spacing out these standing waves in frequency. As a result, the effects of these standing waves are not so apparent in devices with $Q > 10$ as variations in the impedance are small over the response bandwidth of the JPA.

The full "pumpistor" theory,[17] while previously validated for only the degenerate frequency (phase-sensitive) case,[16] is well suited to a detailed analysis of the effect of these standing waves on non-degenerate gain in a JPA. Here, the non-linearity of a flux-pumped SQUID loop is treated as a power dependent modification of the SQUID inductance. For a signal at frequency ω_s, the admittance of the loop

becomes $Y(\omega_s) = 1/i\omega_s L_0 + 1/i\omega_s(L_1 + L_2)$, where the three elements of the inductance are

$$L_0 = L_j/\cos(\pi\Phi_Q/\Phi_0), \tag{1}$$

$$L_1 = -\frac{4L_j\cos(\pi\Phi_Q/\Phi_0)}{\pi^2\sin^2(\pi\Phi_Q/\Phi_0)}\left(\frac{\Phi_0}{\Phi_{ac}}\right)^2, \tag{2}$$

$$L_2 = i\frac{4\omega_i L_j^2 Y^\star_{\rm ext}(\omega_i)}{\pi^2\sin^2(\pi\Phi_Q/\Phi_0)}\left(\frac{\Phi_0}{\Phi_{ac}}\right)^2. \tag{3}$$

Here, the idler frequency $\omega_i = \omega_p - \omega_s$, $L_j = \Phi_0/(2\pi I_c)$ is the unbiased SQUID inductance, Φ_Q is the DC flux bias, and Φ_{ac} is the amplitude of the flux pump. The dependence of L_2 on the external admittance at the idler frequency $Y^\star_{\rm ext}(\omega_i)$ comes about because the pump also drives oscillations at the idler frequency, and the magnitude of these oscillations depends on the output admittance. As the pump power increases from zero, $L_1 + L_2$ emerges as an element in parallel with the initial SQUID inductance L_0. The term L_1 modifies the inductance of the circuit, lowering the operating frequency as pump power increases. The term L_2 represents an imaginary inductance that gives rise to a negative real impedance given by $\mathrm{Re}[i\omega_s L_2]$.

As the JPA is a reflection amplifier, we can use our "pumpistor" model to calculate the reflection coefficient and thus the gain G using the admittance (impedance) mismatch between the external environment $Y_{\rm ext}$ and the paramp admittance $Y_{\rm JPA}$.

$$G(\omega_s) = \frac{Y_{\rm ext}(\omega_s) - Y_{\rm JPA}(\omega_s)}{Y_{\rm ext}(\omega_s) + Y_{\rm JPA}(\omega_s)}. \tag{4}$$

Using Eqs. (1)–(3), we derive a simplified approximation of the JPA admittance which includes the SQUID loop and shunt capacitance C

$$Y_{\rm JPA}(\omega_s) = \frac{-2i(\omega_o - \omega_s)}{\omega_o\omega_s L_c} - \frac{\pi^2\sin^2(\pi\Phi_Q/\Phi_0)(\Phi_{ac}/\Phi_0)^2}{4\alpha\omega_s\omega_i L_j^2 Y^\star_{\rm ext}(\omega_i)}, \tag{5}$$

where $1/L_c = 1/L_0 + 1/L_1$ is the combined parallel inductance of the SQUID, $\omega_o = 1/\sqrt{CL_c} \approx \omega_p/2$, and $\alpha = 1 + Q^2 \approx 10$ is due to a series to parallel circuit conversion.[23] Equations (4) and (5) describe how a knowledge of the frequency dependent admittance of the environment at both the signal and idler frequencies is required to model amplifier behavior.

We show, in Fig. 3(a), solutions to Eqs. (4) and (5) with a 10% sinusoidal variation in $Y_{\rm ext}$. With increasing power, the denominator in Eq. (4) is brought closer to zero, resulting in increased gain. The $Q = 20$ case shows that the effect of $Y_{\rm ext}$ on the overall gain is dominated by the narrowed response of the JPA. For comparison, in the $Q = 3$ case (gold, light), the response of the JPA is broad enough to sample variations in the external environment. Moreover, the profile of the gain reflects the shape of $Y_{\rm ext}$ at that frequency. This results in the variations in bandwidth seen in the left versus right simulation. We note that the measured gain profiles show a high degree of symmetry for ω_s about $\omega_p/2$, regardless of the detailed behavior of $Y_{\rm ext}$. This is to be expected, as the gain samples $Y_{\rm ext}$ at both the signal and idler frequencies, which are symmetrically placed about $\omega_p/2$. A broader sampling of frequency dependent gain profiles calculated using Eqs. (4) and (5) are shown in Ref. 23 with a similar degree of symmetry.

To test the dependence of amplifier performance on environment admittance, we changed the pattern of standing waves on the output line by changing the length of cable separating the device from the circulator. We measured the gains as a function of ω_s for different resonant frequencies ω_o from 5 to 7 GHz with direct connection to the circulator,

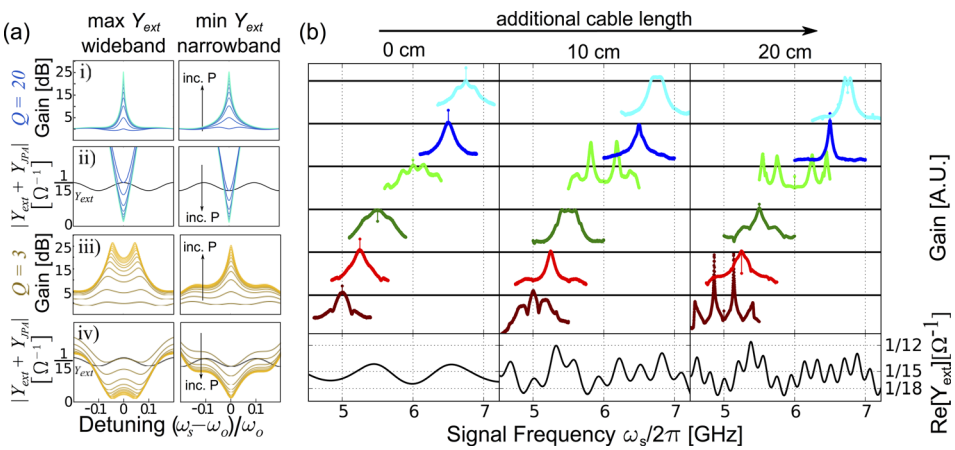

FIG. 3. Effect of variation in external admittance on amplifier performance. (a) Simulated gain profiles ((i) and (iii)) showing the effect of external impedance on gain for both weak ($Q = 20$) and strong ($Q = 3$) coupling. Higher pump power is denoted by lighter colored traces and indicated by the arrow. The denominator of Eq. (4) ((ii) and (iv)) is plotted, with the gain shown in (i) and (iii). As pump power increases the denominator is displaced from $Y_{\rm ext}$ towards zero by an increasingly negative $Y_{\rm JPA}$. In a weakly coupled device ((i) and (ii)), the gain profile is not affected by the shape of the external admittance. In the case of strong coupling ((iii) and (iv)), the response of the JPA is broader and the gain profile is greatly influenced by the external admittance. If $\omega_p/2 = \omega_o$ is centered at a maxima in external admittance the gain is broadened (left), if ω_o is centered on a minima it is narrowed (right). (b) Experimental variation of the standing waves in the external environment. Gain profiles of approximately 20 dB, and offset by 20 dB (denoted by bold horizontal lines) are shown as the amplifier frequency ω_o is tuned from 5 to 7 GHz. Standing waves are introduced by lengthening the cable between the IMPA and the circulator; the longer the cable, the more closely spaced in frequency are the standing waves. Amplitude variations in $Y_{\rm ext}$ come from a superposition of standing waves in the cable and on-chip taper. The gain profiles become increasingly featured as the variations in $Y_{\rm ext}$ (calculated using SPICE) increase with cable length.

a 10 cm and 20 cm cable. The results of this experiment are shown in Fig. 3(b). In each case, a series of gain profiles with ~20 dB peak gain are shown, spaced vertically. We also plot the frequency-dependent output admittance taken from simulations using the corresponding length of cable. This frequency-dependent admittance can be estimated using lumped circuit models to approximate the dominant contributions from the circulator and wire-bond connections.

When the amplifier is connected directly to the circulator, the admittance variation is minimized and the IMPA more consistently approaches the expected Lorentzian gain profiles. When connected using the 10 cm cable, a drastic change is exhibited in many of the peaks showing both broadening at some frequencies and narrowing at others. When the 20 cm cable is used, the output impedance varies more rapidly and the device performance becomes increasingly erratic while often exhibiting multiple distinct resonant peaks. The experimental data show good qualitative agreement to that predicted by the "pumpistor" reflection model.

While the gain profile is strongly dependent on frequency, when the amplifier is properly tuned for quantum-limited noise performance the complexity of the gain profile is insensitive to DC flux and pump power. Moreover, we see very little chip to chip and run to run variation, with most of the performance variations arising from changes to the experimental setup. This effect is evident in the nominally Lorentzian gain profiles observed with direct connection to the circulator. This reliability is further demonstrated by the IMPA's use in broadband, high-power, multi-qubit readout in existing experiments.[14,25] These experiments both make use of the operation point shown in Fig. 2 with a roughly 10 cm copper cable connecting the IMPA to the circulator.

In conclusion, we have demonstrated validation of the "pumpistor" theory and application of a new model for understanding parametric amplifier behavior. In the strongly coupled limit this model predicts unexpectedly large bandwidths, which have been observed in the IMPA with near quantum-limited noise performance. Using this model, further improvements should be possible by shaping the external embedding impedance, possibly with alternate matching networks.[26] Additionally, this strong coupling could enhance performance in alternate JPA designs, such as multi-SQUID JPA.[20] This large bandwidth, along with a significant increase in saturation power, has allowed us to study high power measurement in a multi-qubit device,[25] suitable for error correction architectures.[13,14]

This work was supported by the Office of the Director of National Intelligence (ODNI), Intelligence Advanced Research Projects Activity (IARPA), through the Army Research Office Grant No. W911NF-10-1-0334. All statements of fact, opinion or conclusions contained herein are those of the authors and should not be construed as representing the official views or policies of IARPA, the ODNI, or the U.S. Government. Devices were made at the UC Santa Barbara Nanofabrication Facility, a part of the NSF funded National Nanotechnology Infrastructure Network, and at the NanoStructures Cleanroom Facility.

[1]C. M. Caves, Phys. Rev. D **26**, 1817 (1982).
[2]P. Kumar, O. Aytür, and J. Huang, Phys. Rev. Lett. **64**, 1015 (1990).
[3]S. J. Asztalos, G. Carosi, C. Hagmann, D. Kinion, K. Van Bibber, M. Hotz, L. Rosenberg, G. Rybka, J. Hoskins, J. Hwang *et al.*, Phys. Rev. Lett. **104**, 041301 (2010).
[4]A. Wallraff, D. Schuster, A. Blais, L. Frunzio, J. Majer, M. Devoret, S. Girvin, and R. Schoelkopf, Phys. Rev. Lett. **95**, 060501 (2005).
[5]B. Yurke, L. Corruccini, P. Kaminsky, L. Rupp, A. Smith, A. Silver, R. Simon, and E. Whittaker, Phys. Rev. A **39**, 2519 (1989).
[6]T. Yamamoto, K. Inomata, M. Watanabe, K. Matsuba, T. Miyazaki, W. Oliver, Y. Nakamura, and J. Tsai, Appl. Phys. Lett. **93**, 042510 (2008).
[7]M. Castellanos-Beltran and K. Lehnert, Appl. Phys. Lett. **91**, 083509 (2007).
[8]M. Hatridge, R. Vijay, D. Slichter, J. Clarke, and I. Siddiqi, Phys. Rev. B **83**, 134501 (2011).
[9]B. Abdo, F. Schackert, M. Hatridge, C. Rigetti, and M. Devoret, Appl. Phys. Lett. **99**, 162506 (2011).
[10]J. Mutus, T. White, E. Jeffrey, D. Sank, R. Barends, J. Bochmann, Y. Chen, Z. Chen, B. Chiaro, A. Dunsworth *et al.*, Appl. Phys. Lett. **103**, 122602 (2013).
[11]R. Vijay, D. Slichter, and I. Siddiqi, Phys. Rev. Lett. **106**, 110502 (2011).
[12]M. Hatridge, S. Shankar, M. Mirrahimi, F. Schackert, K. Geerlings, T. Brecht, K. Sliwa, B. Abdo, L. Frunzio, S. Girvin *et al.*, Science **339**, 178 (2013).
[13]A. G. Fowler, M. Mariantoni, J. M. Martinis, and A. N. Cleland, Phys. Rev. A **86**, 032324 (2012).
[14]R. Barends, J. Kelly, A. Megrant, D. Sank, E. Jeffrey, Y. Chen, Y. Yin, B. Chiaro, J. Mutus, C. Neill *et al.*, Nature **508**, 500 (2014).
[15]P. K. Day, H. G. LeDuc, B. A. Mazin, A. Vayonakis, and J. Zmuidzinas, Nature **425**, 817 (2003).
[16]K. Sundqvist, S. Kintas, M. Simoen, P. Krantz, M. Sandberg, C. Wilson, and P. Delsing, Appl. Phys. Lett. **103**, 102603 (2013).
[17]K. M. Sundqvist and P. Delsing, EPJ Quantum Technology **1**(1), 6 (2014).
[18]R. Bradley, Nucl. Phys. B, Proc. Suppl. **72**, 137 (1999).
[19]V. Manucharyan, E. Boaknin, M. Metcalfe, R. Vijay, I. Siddiqi, and M. Devoret, Phys. Rev. B **76**, 014524 (2007).
[20]C. Eichler and A. Wallraff, EPJ Quantum Technology **1**(1), 1 (2014).
[21]R. Klopfenstein, Proc. IRE **44**, 31 (1956).
[22]D. M. Pozar, *Microwave Engineering* (John Wiley & Sons, 2009).
[23]See supplementary material at http://dx.doi.org/10.1063/1.4886408 for full description of device fab, characterization, and mathematical approximations.
[24]I. Siddiqi, R. Vijay, F. Pierre, C. Wilson, M. Metcalfe, C. Rigetti, L. Frunzio, and M. Devoret, Phys. Rev. Lett. **93**, 207002 (2004).
[25]E. Jeffrey, D. Sank, R. Barends, J. Kelly, A. Megrant, Y. Chen, Y. Yin, B. Chiaro, J. Mutus, C. Neill *et al.*, Phys. Rev. Lett. **112**, 190504 (2014).
[26]L. Ranzani, L. Spietz, Z. Popovic, and J. Aumentado, IEEE Trans. Appl. Supercond. **22**, 1500606 (2012).